Supporting Information

Enhancing persistent radioluminescence in perovskite scintillators through trap defect modulation

Xiaokun Li[1, †], Huixi Guo[2, 3, †], Yahuang Li[1], Caihou Lin[4, *], Lili Xie[1, *]

1.Department of Health Inspection and Quarantine, School of Public Health, Fujian Medical University, Fuzhou, 350122, Fujian, China
Email: 1006xielili@fjmu.edu.cn
2.Department of Gastroenterology, Shengli Clinical Medical College of Fujian Medical University, Fuzhou, Fujian, China
3.Department of Gastroenterology, Fujian Provincial Hospital, Fuzhou, Fujian, China
4. Department of Neurosurgery, Union Hospital Affiliated of Fujian Medical University, Fuzhou 350001, Fujian, China
Email: grouplin@fjmu.edu.cn
[†]These authors have contributed equally to this work.

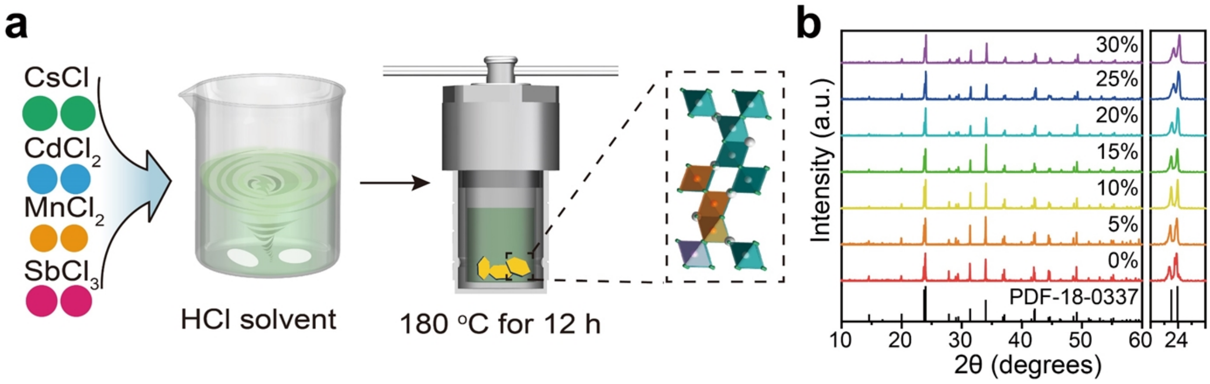

Figure S1. Synthesis and characterization of crystal. (a) Schematic for the synthesis of $CsCdCl_3$:Mn^{2+}/Sb^{3+} crystal. **(b)** XRD patterns of $CsCdCl_3$ powder with different Mn^{2+} doping concentrations.

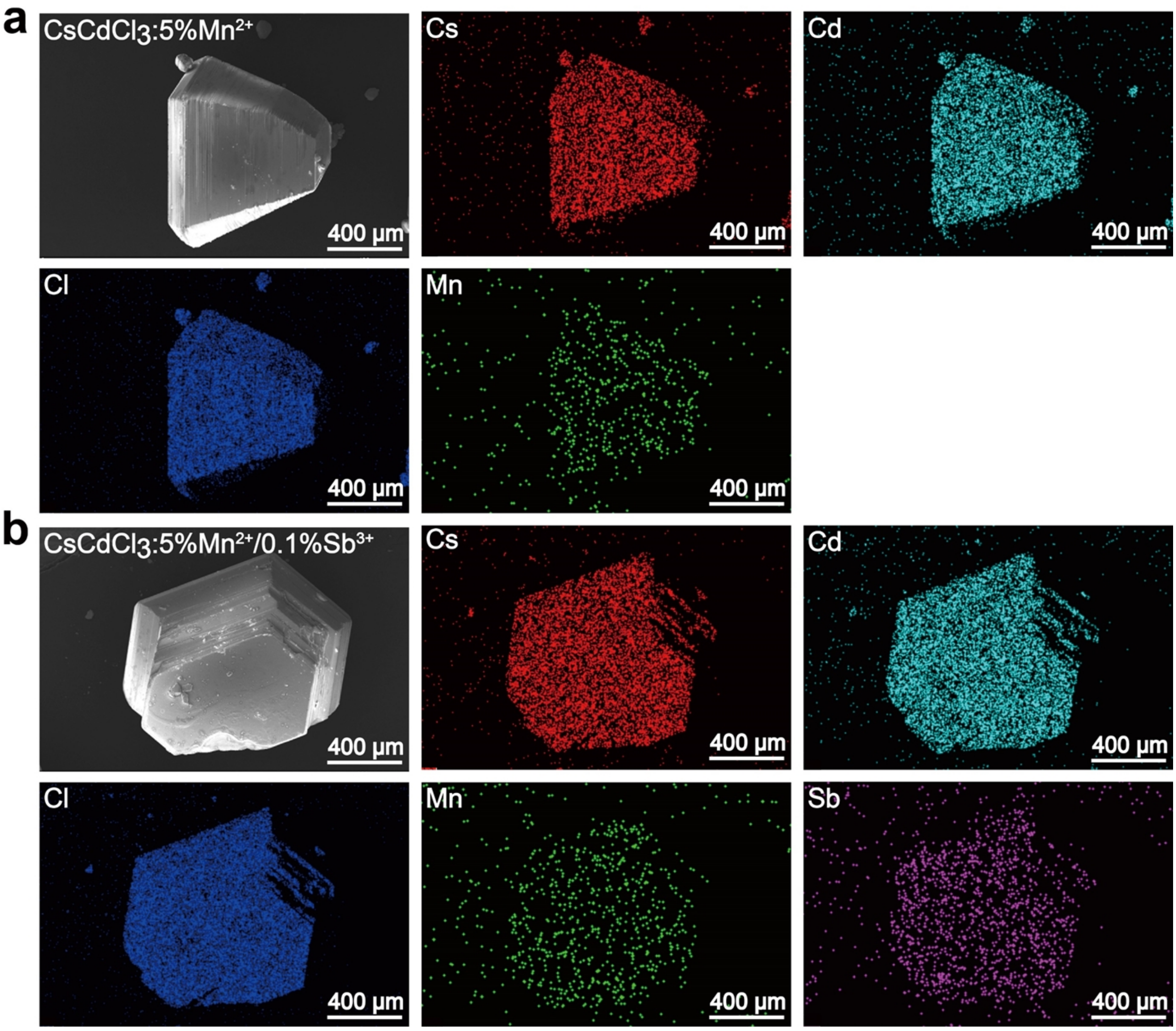

Figure S2. Chemical composition analysis of crystal. SEM images of $CsCdCl_3$:5%Mn^{2+} (a) and $CsCdCl_3$:5%Mn^{2+}/0.1%Sb^{3+}(b), and corresponding elemental maps of Cs, Cd, Cl, Mn and Sb.

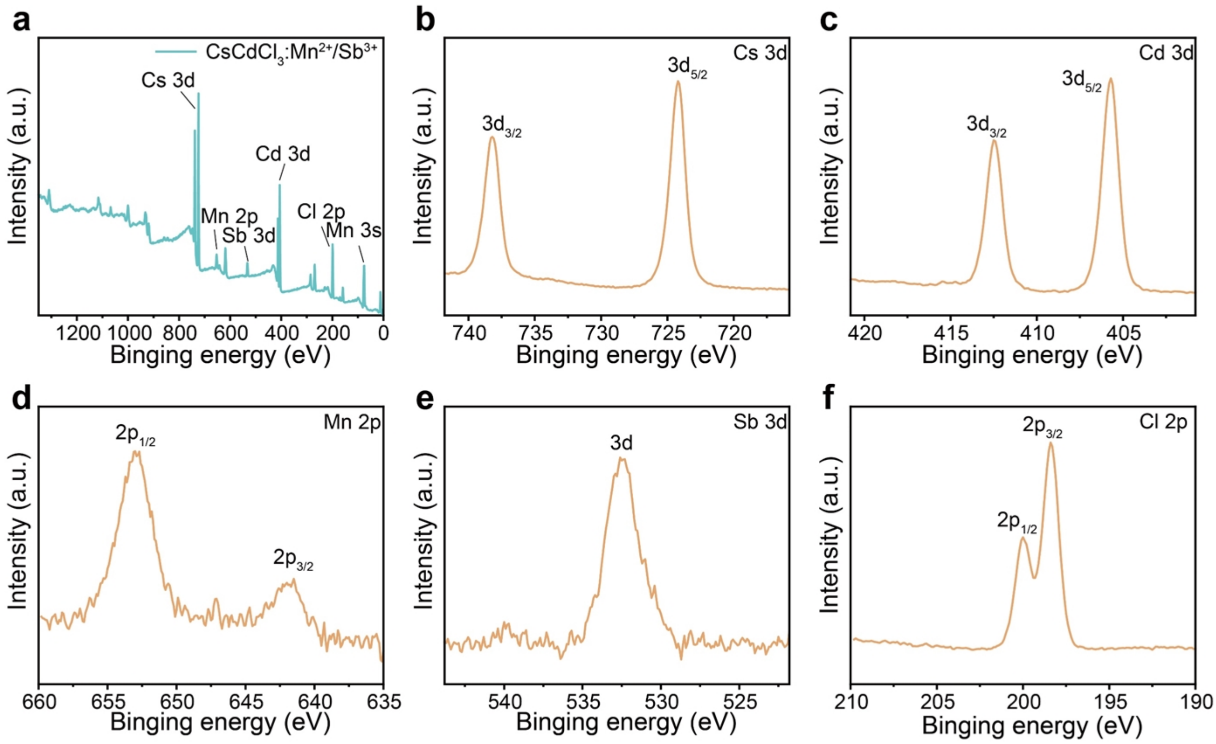

Figure S3. X-ray photoelectron spectroscopy of $CsCdCl_3$:5%Mn^{2+}/0.1%Sb^{3+}. (a) XPS spectra of $CsCdCl_3$:5%Mn^{2+}/0.1%Sb^{3+}. **(b-f)** The corresponding high-resolution XPS spectra of Cs 3d, Cd 3d, Mn 2p, Sb 3d, and Cl 2p.

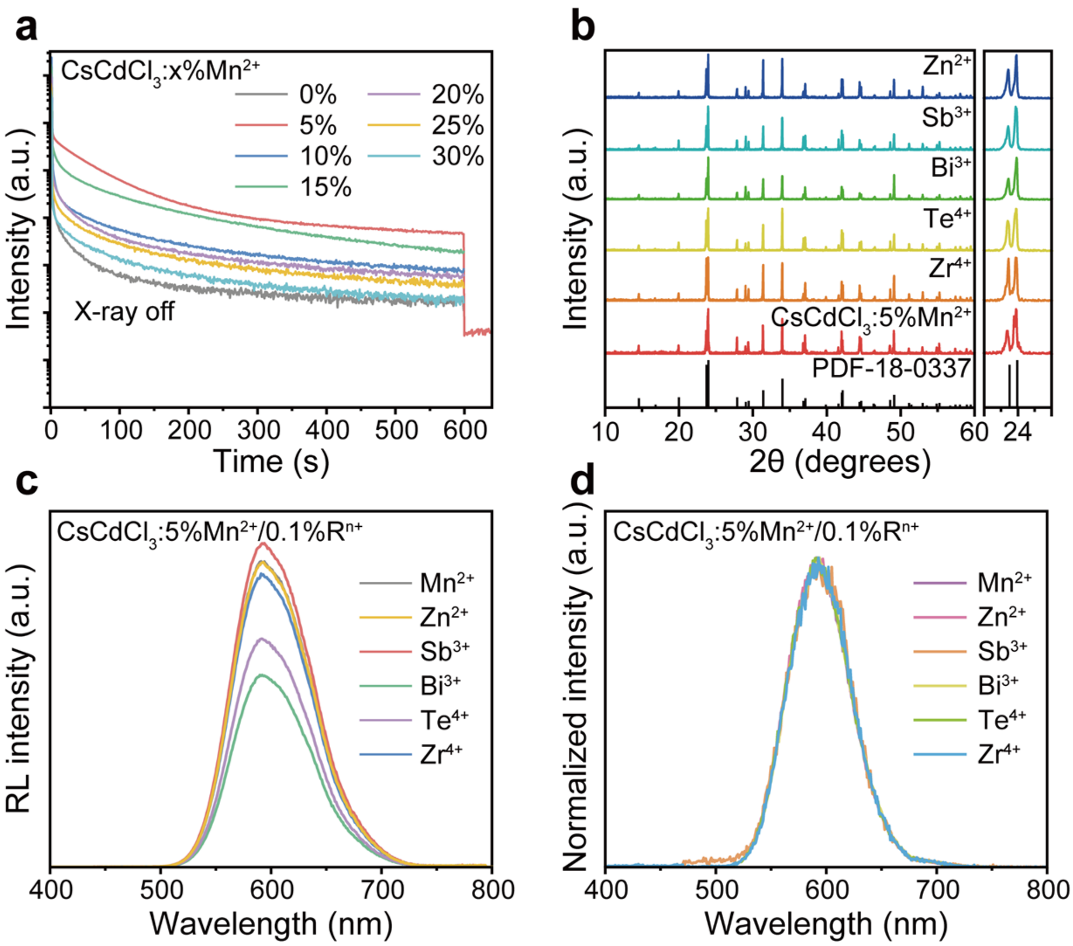

Figure S4. Structural characterization and optical investigation of $CsCdCl_3$ crystal with different doping concentrations and ions. (a) Afterglow decay curve of $CsCdCl_3$:x%Mn^{2+} (x = 0-30%) at room temperature after cessation of X-ray excitation (50 kV, 3 min). **(b)** XRD patterns of $CsCdCl_3$:5%Mn^{2+} powder with different doping ions. **(c).** Radioluminescence spectra of $CsCdCl_3$:5%Mn^{2+}/0.1%R^{n+} crystals. **(d).** Photoluminescence spectra of $CsCdCl_3$:5%Mn^{2+}/0.1%R^{n+} crystals.

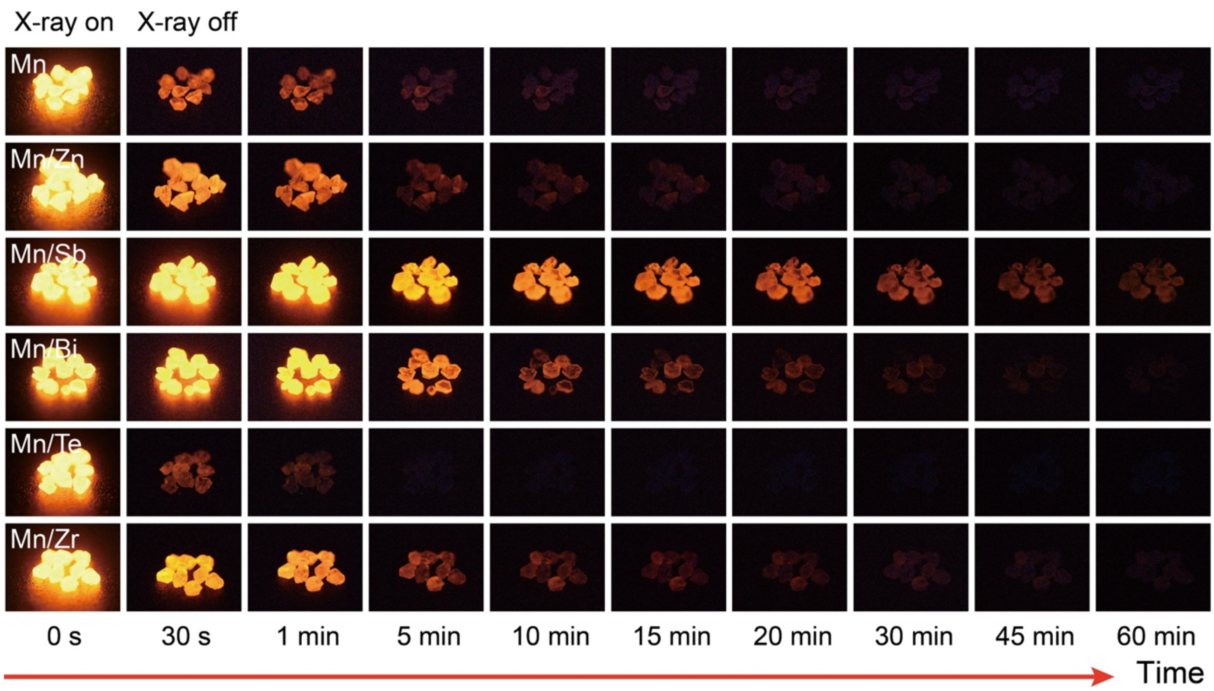

Figure S5. The radioluminescence afterglow decay characteristics of $CsCdCl_3$:5%Mn^{2+} with different doping ions. Afterglow photographs of crystals taken under X-ray excitation and at different times after the removal of X-ray.

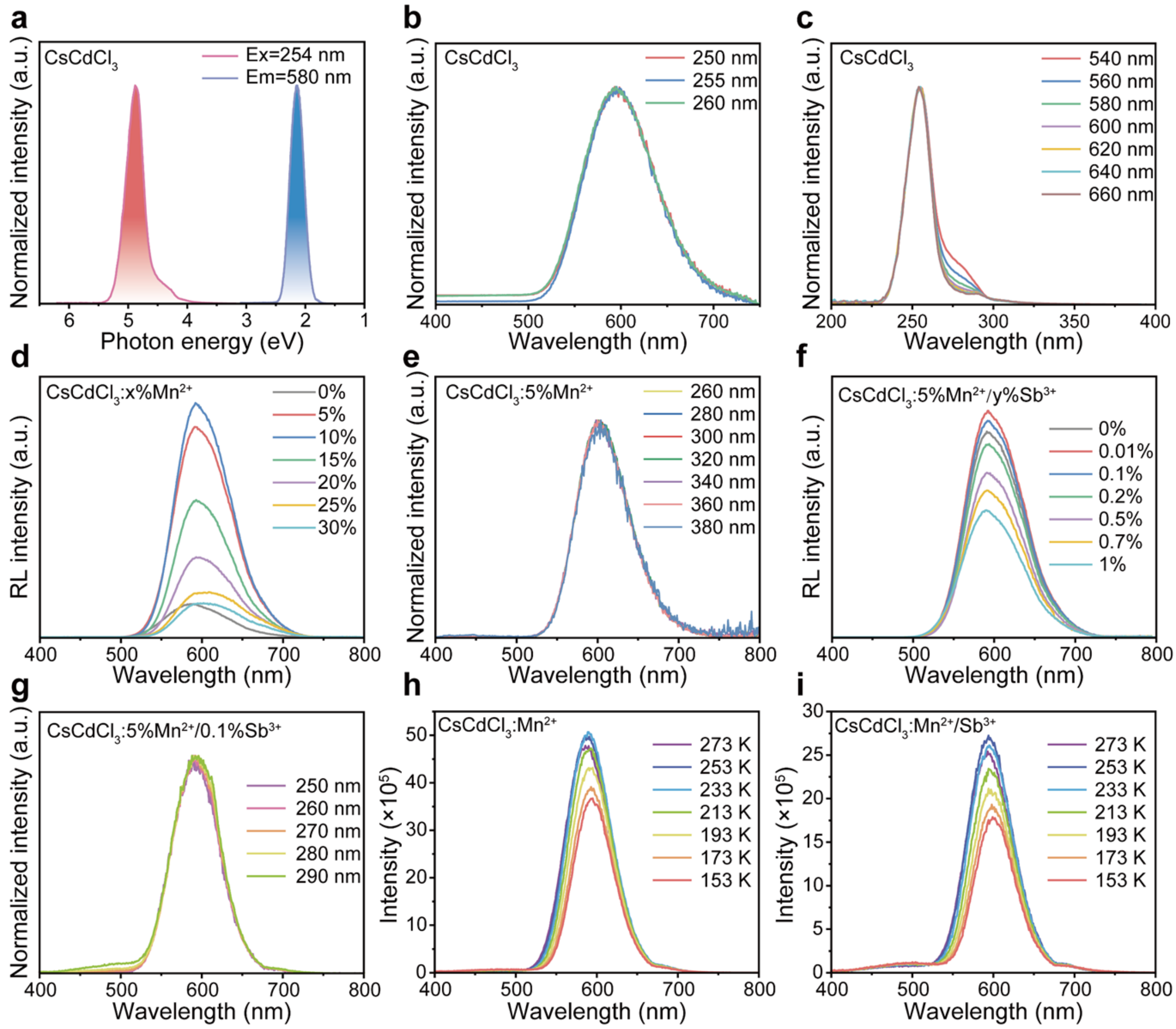

Figure S6. Optical characterization and mechanism investigation of $CsCdCl_3$ crystal with different doping concentrations and ions. (a) Excitation and emission spectra of the $CsCdCl_3$ crystals. (b) Photoluminescence spectra at different excitation wavelengths of $CsCdCl_3$ crystals. (c) Photoluminescence excitation spectra at different emission wavelengths of $CsCdCl_3$. (d) Radioluminescence spectra of $CsCdCl_3$:x%Mn^{2+} (x = 0-30%) crystals. (e) Photoluminescence spectra at different excitation wavelengths of $CsCdCl_3$:5%Mn^{2+}. (f) Radioluminescence spectra of $CsCdCl_3$:5%Mn^{2+}/y% Sb^{3+} (y = 0-1%) crystals. (g) Photoluminescence spectra at different excitation wavelengths of $CsCdCl_3$:5%Mn^{2+}/0.1%Sb^{3+}. (h) Low temperature-dependent photoluminescence spectra of $CsCdCl_3$:5%Mn^{2+}. (i) Low temperature-dependent photoluminescence spectra of $CsCdCl_3$:5%Mn^{2+}/0.1%Sb^{3+}**.**

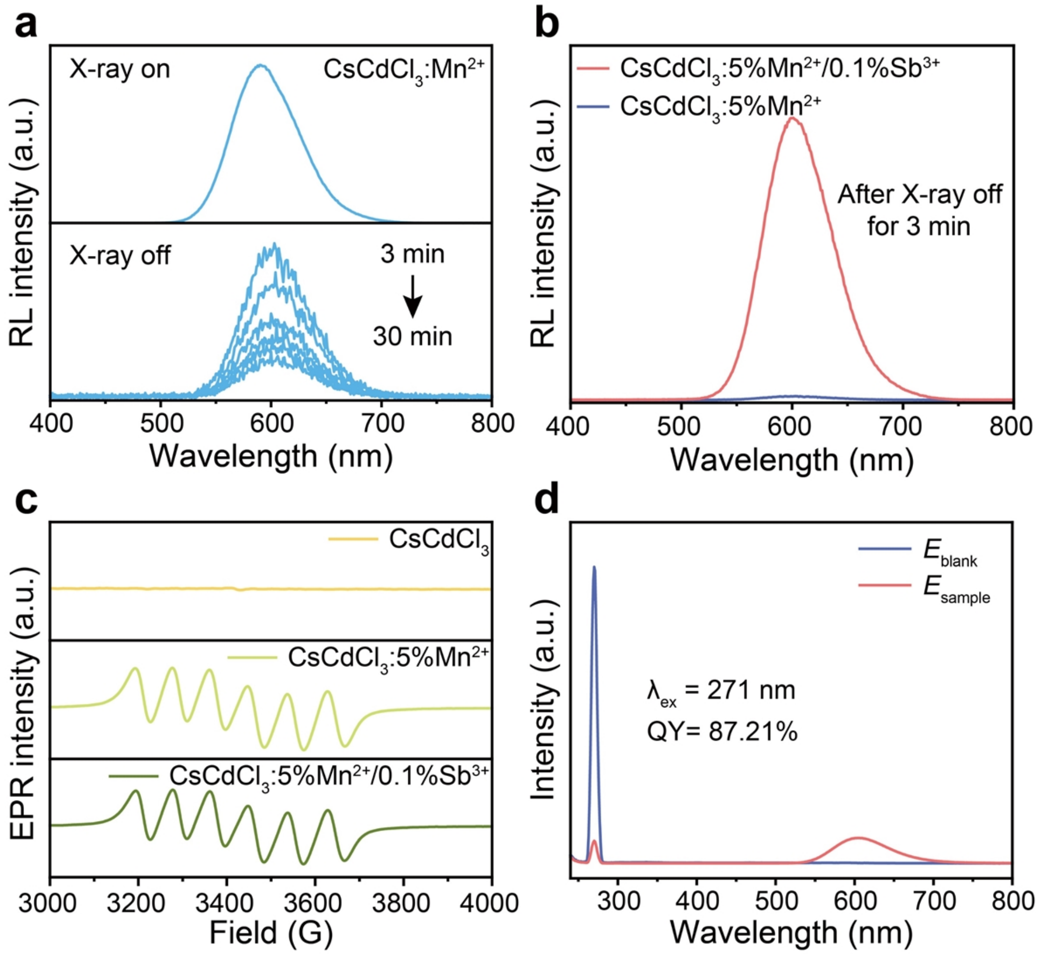

Figure S7. Effect of doped ions on luminescent properties and persistent Luminescent properties. (a) Radioluminescence spectra of $CsCdCl_3$:5%Mn^{2+} crystals within 30 min at room temperature after cessation of X-ray excitation (50 kV, 3 min). (b) Comparison of radioluminescence spectra of $CsCdCl_3$:5%Mn^{2+} and $CsCdCl_3$:5%Mn^{2+}/0.1%Sb^{3+} within 3 min at room temperature after cessation of X-ray excitation (50 kV, 3 min). (c) The evolution of EPR spectra of $CsCdCl_3$, $CsCdCl_3$:5%Mn^{2+} and $CsCdCl_3$:5%Mn^{2+}/0.1%Sb^{3+}. (d) Photoluminescence quantum yield (PLQY) of $CsCdCl_3$:5%Mn^{2+}/0.1%Sb^{3+} crystal.

Table S1: Experiment mole ratio and actual doping concentration of Mn^{2+} in $CsCdCl_3$:x%Mn^{2+}.

Samples / $CsCdCl_3$:x%Mn^{2+}	1	2	3	4	5	6
Doping ion	Mn^{2+}	Mn^{2+}	Mn^{2+}	Mn^{2+}	Mn^{2+}	Mn^{2+}
Theoretical doping concentration	5%	10%	15%	20%	25%	30%
Actual doping concentration	4.2474%	9.8522%	13.2982%	19.2661%	24.4095%	28.3591%
mass fraction	0.6592%	1.5159%	2.0353%	2.9220%	3.6734%	4.2425%

Table S2: Experiment mole ratio and actual doping concentration of Mn^{2+} and Sb^{3+} in $CsCdCl_3$:x%Mn^{2+}/y%Sb^{3+}.

Samples $CsCdCl_3$:x%Mn^{2+}/y%Sb^{3+}	1	2	3	4	5	6
Doping ion	Mn^{2+}	Mn^{2+}	Mn^{2+}	Mn^{2+}	Mn^{2+}	Mn^{2+}
Theoretical doping concentration	5%	5%	5%	5%	5%	5%
Actual doping concentration	4.6029%	4.4898%	4.4283%	4.5369%	4.9482%	4.6796%
mass fraction	0.7139%	0.6963%	0.6866%	0.7026%	0.7654%	0.7235%
Doping ion	Sb^{3+}	Sb^{3+}	Sb^{3+}	Sb^{3+}	Sb^{3+}	Sb^{3+}
Theoretical doping concentration	0.01%	0.1%	0.2%	0.5%	0.7%	1%
Actual doping concentration	0.0157%	0.0975%	0.1808%	0.4964%	0.6423%	0.9205%
mass fraction	0.0054%	0.0335%	0.0621%	0.1704%	0.2202%	0.3154%

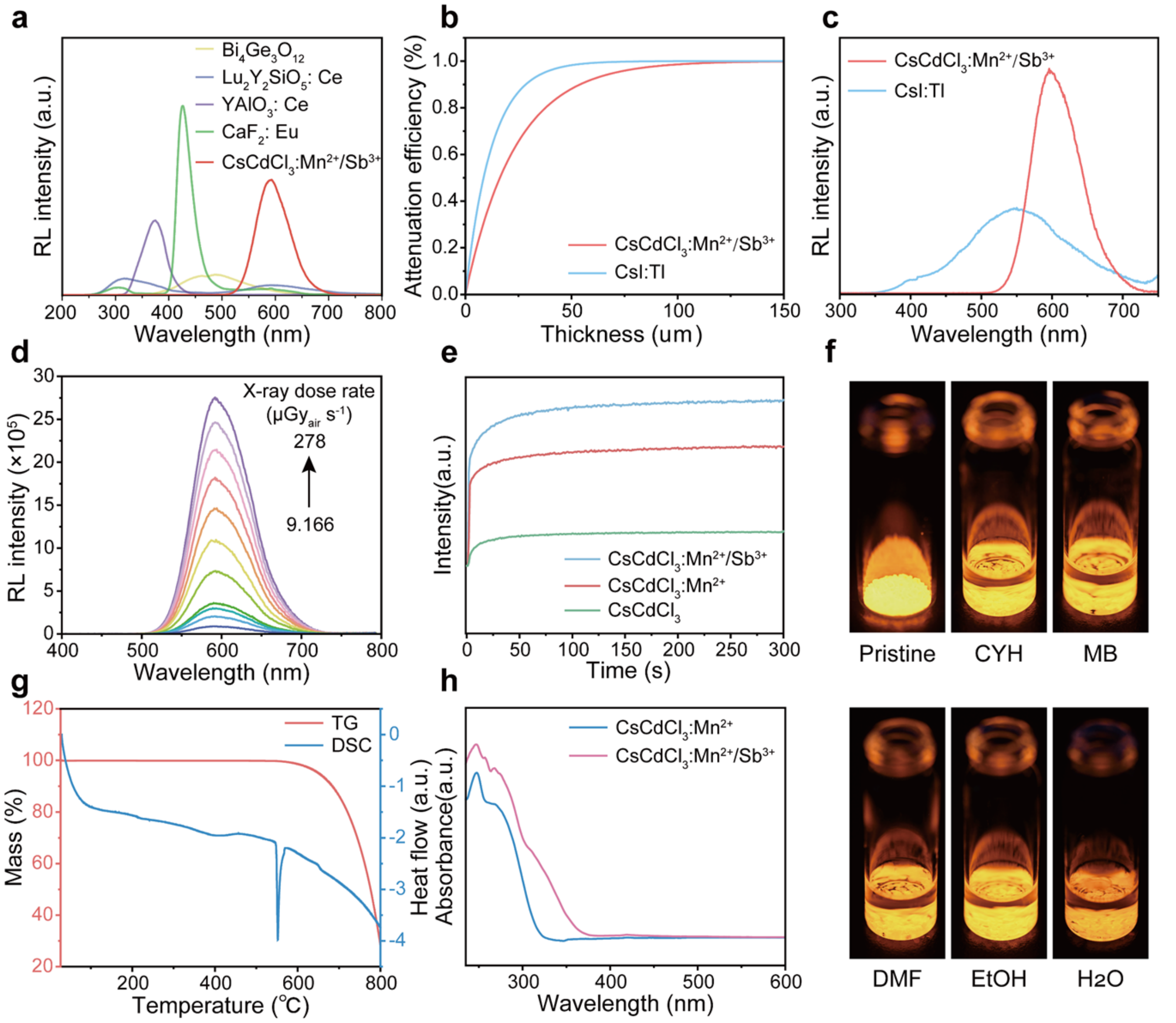

Figure S8. Photophysical investigations of X-ray irradiation on $CsCdCl_3$:5%Mn^{2+}/0.1%Sb^{3+} crystals. (a) Radioluminescence spectra of $CsCdCl_3$:5%Mn^{2+}/0.1%Sb^{3+} and commercial inorganic scintillator materials. (b) Calculated X-ray attention efficiencies of CsI:Tl and $CsCdCl_3$:Mn^{2+}/Sb^{3+} crystals. (c) Comparison of radioluminescence intensity of CsI:Tl and $CsCdCl_3$:Mn^{2+}/Sb^{3+} crystals. (d) Radioluminescence spectra of $CsCdCl_3$:5%Mn^{2+}/0.1%Sb^{3+} in response to X-ray dose rate of 9.166-278 μGy s^{-1}. (e) The radioluminescence intensity of $CsCdCl_3$, $CsCdCl_3$:5%Mn^{2+} and $CsCdCl_3$:5%Mn^{2+}/0.1%Sb^{3+} at 592 nm as a function of time under continuous X-ray irradiation. (f) Radioluminescence photographs of $CsCdCl_3$:5%Mn^{2+}/0.1%Sb^{3+} crystals soaked in different solvents under X-ray irradiation. (g) TGA and DSC curves of $CsCdCl_3$:5%Mn^{2+}/0.1%Sb^{3+}. (h) Absorption spectra of $CsCdCl_3$:5%Mn^{2+} and $CsCdCl_3$:5%Mn^{2+}/0.1%Sb^{3+}.

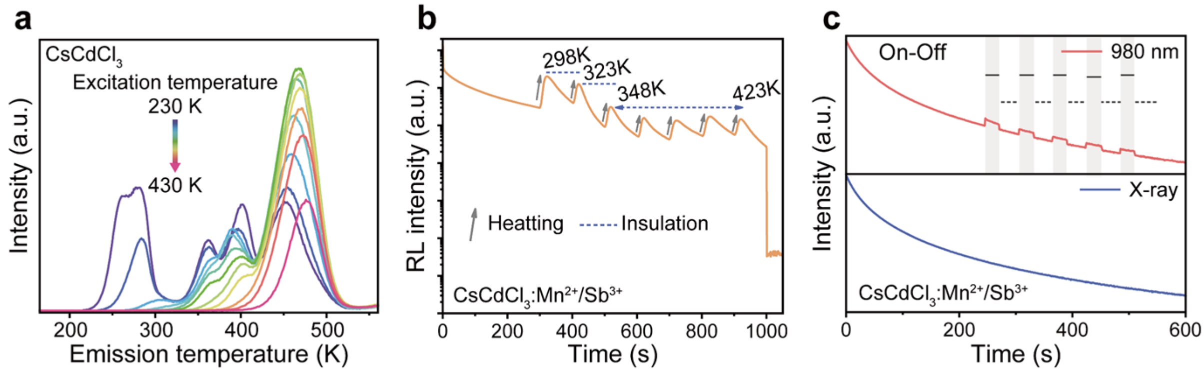

Figure S9. Characterization of energy trap in $CsCdCl_3$ crystals. (a) Thermoluminescence glow curves of $CsCdCl_3$ in the temperature range of 230 to 430 K after cessation of X-ray excitation (50 kV, 3 min). The heating rate is 60 K/min. (b) TSL decay curves of $CsCdCl_3$:5%Mn^{2+}/0.1%Sb^{3+} under thermal stimulation with different temperatures after cessation of X-ray excitation (50 kV, 3 min). (c) Comparison of radioluminescence decay curves of $CsCdCl_3$:5%Mn^{2+}/0.1%Sb^{3+} after X-ray excitation for 3 min (50 kV) and that of repeated light stimulation with 980 nm laser.

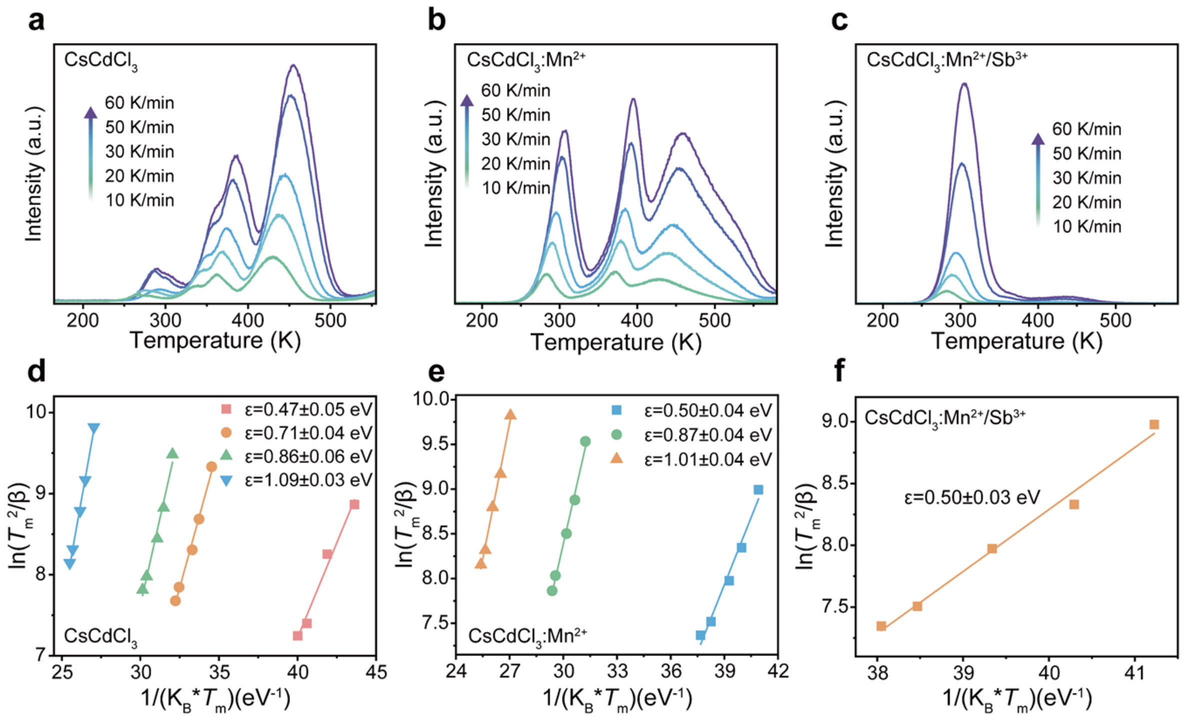

Figure S10. Calculation of trap depth by using the Hoogenstraaten method. (a-c) Thermoluminescence glow curves of $CsCdCl_3$, $CsCdCl_3$:5%Mn^{2+} and $CsCdCl_3$:5%Mn^{2+}/0.1%Sb^{3+} measured with different heating rates (β) of 10, 20, 30, 50, and 60 K/min after X-ray irradiation. (d-f) The corresponding defect depth fitting results were determined by Hoogenstraaten method.

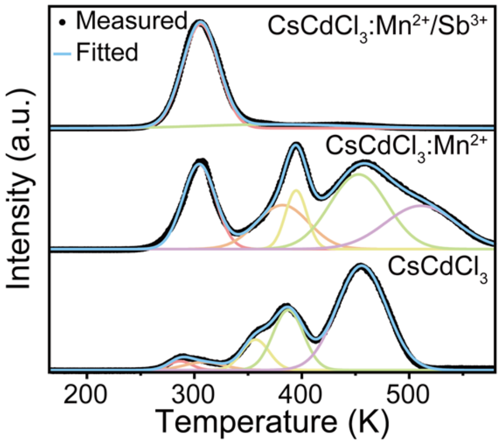

Figure S11. Calculation of trap density. Deconvolution of thermoluminescence glow curves of $CsCdCl_3$, $CsCdCl_3$:5%Mn^{2+} and $CsCdCl_3$:5%Mn^{2+}/0.1%Sb^{3+} measured measured at a heating rate of 60 K/min after X-ray irradiation.

Table S3. Parameters of the thermoluminescence glow curves of $CsCdCl_3$, $CsCdCl_3$:5%Mn^{2+} and $CsCdCl_3$:5%Mn^{2+}/0.1%Sb^{3+} at 270 k for calculate the trap density.

Samples	Peak	T_m(K)	ω	I_m	μ_g	β (K/min)	n
$CsCdCl_3$	Peak1	286.96	29.86	13534.18	0.50	60	121147.76
	Peak2	309.29	51.66	12470.24	0.50	60	193106.70
	Peak3	357.00	31.35	39653.46	0.50	60	372599.18
	Peak4	387.44	34.42	75622.73	0.50	60	780233.47
	Peak5	455.72	55.35	129302.25	0.50	60	2145175.93
$CsCdCl_3:Mn^{2+}$	Peak1	304.54	35.81	90309.30	0.50	60	969465.18
	Peak2	382.00	58.29	47498.58	0.50	60	829878.79
	Peak3	394.73	23.83	62846.73	0.50	60	448928.75
	Peak4	453.00	63.61	79704.99	0.50	60	1519742.92
	Peak5	511.00	79.72	46841.50	0.50	60	1119389.48
$CsCdCl_3:Mn^{2+}/Sb^{3+}$	Peak1	305.99	39.60	167565.09	0.50	60	1989289.98
	Peak2	376.00	163.89	6501.85	0.50	60	319418.90

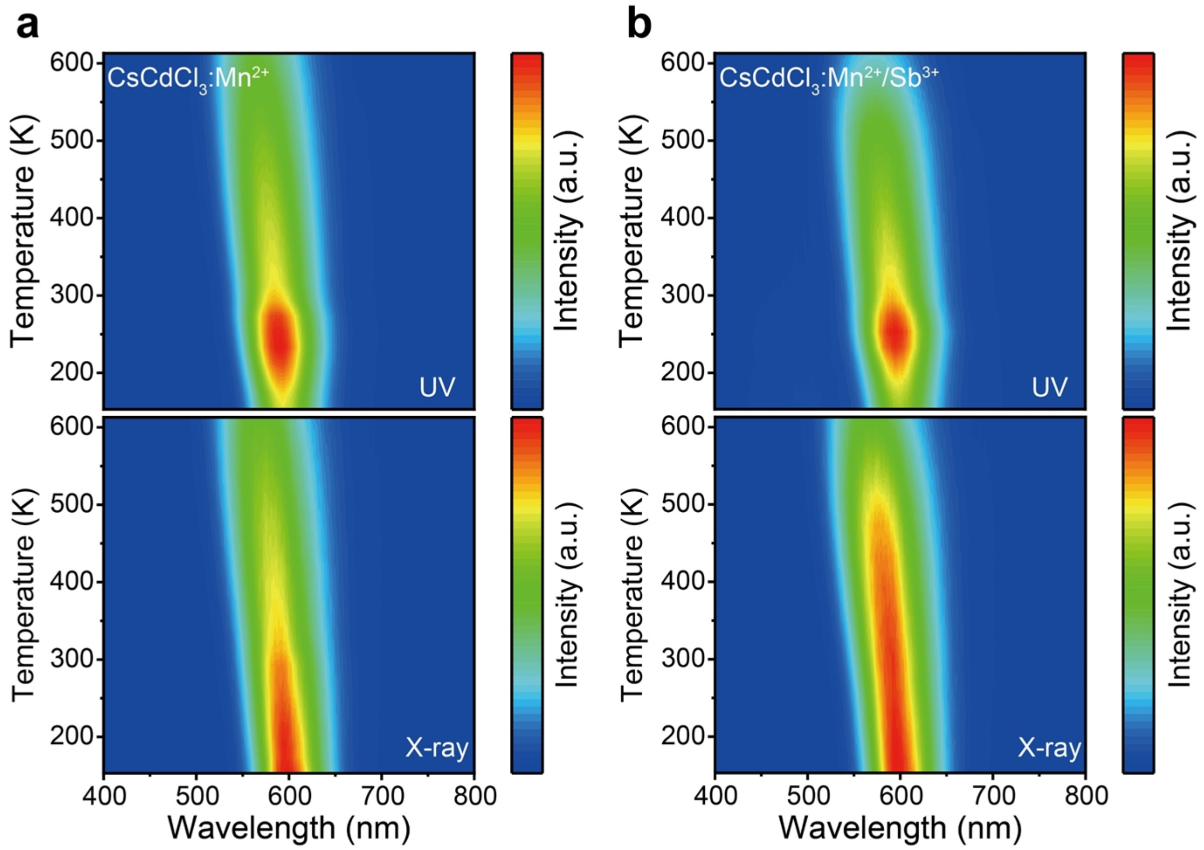

Figure S12. Temperature-dependent spectra. (a-b) Luminescence intensity of $CsCdCl_3$:5%Mn^{2+} and $CsCdCl_3$:5%Mn^{2+}/0.1%Sb^{3+} as a function of emission wavelength and temperature from 153 to 613 K under X-ray and UV excitation.

Table S4: The calculated lattice constant α_0, bulk modulus B, pressure derivative B_0, elastic constants C_{11}, C_{12}, C_{44}, shear modulus G, shear wave modulus Cs, Young's modulus E, Kleinman parameter (ζ), and Poisson's ratio σ at zero pressure.

	Present work		Experiment	Other works
	GGA	LDA		
$\alpha_0(Å)$	5.3107	5.125	[a]5.210	[a]5.289, [b]5.32
$B_0(GPa)$	30.81	42.94	-	-
B'	4.74	4.83	-	-
C_{11}	53.75	79.08	-	-
C_{12}	19.77	25.38	-	-
C_{44}	12.52	14.28	-	-
ζ	0.51	0.47	-	-
G	14.15	18.43	-	-
E	36.85	48.43	-	-
σ	0.302	0.31	-	-
C_S	16.99	26.85	-	-

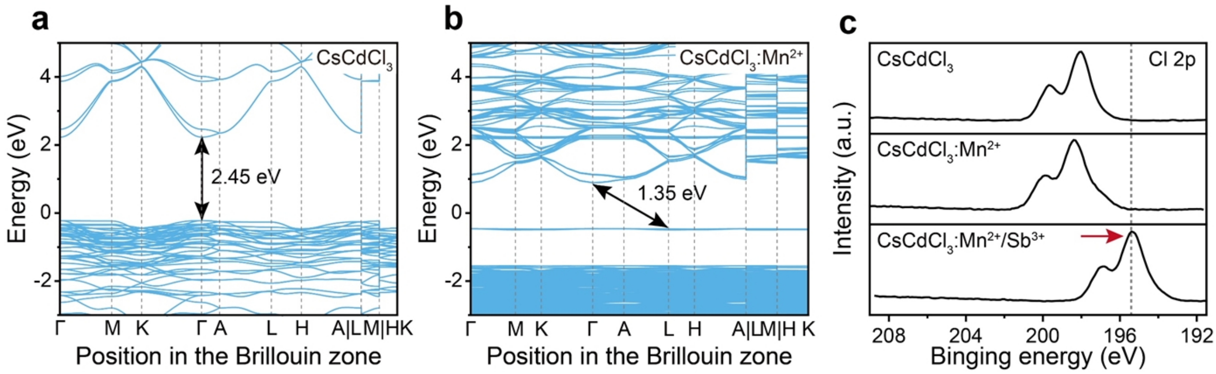

Figure S13. Investigation of band structures and traps in $CsCdCl_3$. (a-b) Calculated band structure of $CsCdCl_3$ and $CsCdCl_3$:5%Mn^{2+}. (c) High-resolution XPS spectra corresponding to Cl 2p of $CsCdCl_3$, $CsCdCl_3$:5%Mn^{2+} and $CsCdCl_3$:5%Mn^{2+}/0.1%Sb^{3+}.

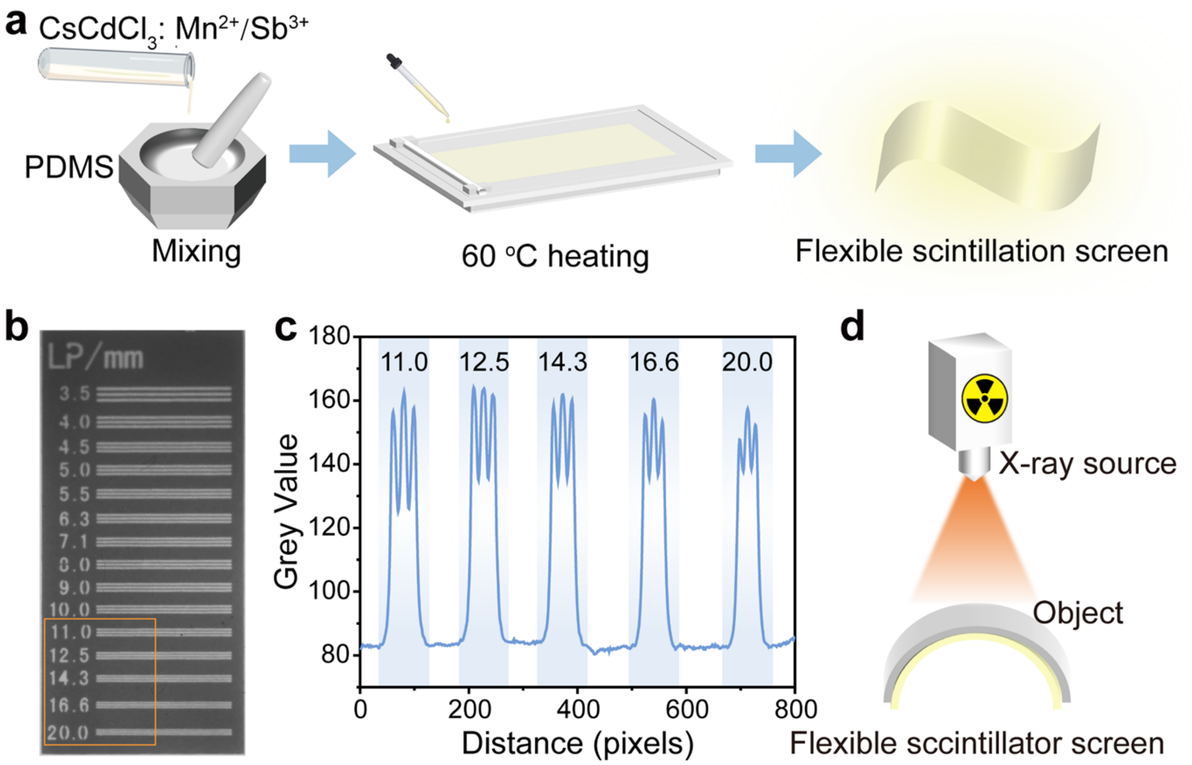

Figure S14. Fabrication of flexible scintillation screen and time-delay imaging. (a) Schematic preparation of $CsCdCl_3$:5%Mn^{2+}/0.1%Sb^{3+} to prepare flexible PDMS scintillator screens. (b) The X-ray image resolution of the $CsCdCl_3$:5%Mn^{2+}/0.1%Sb^{3+} PDMS scintillator screens was measured by the standard X-ray test pattern plate. (c) The intensity was measured by spatial resolution with Gaussian function. (d) Schematic diagram of imaging the curved object.

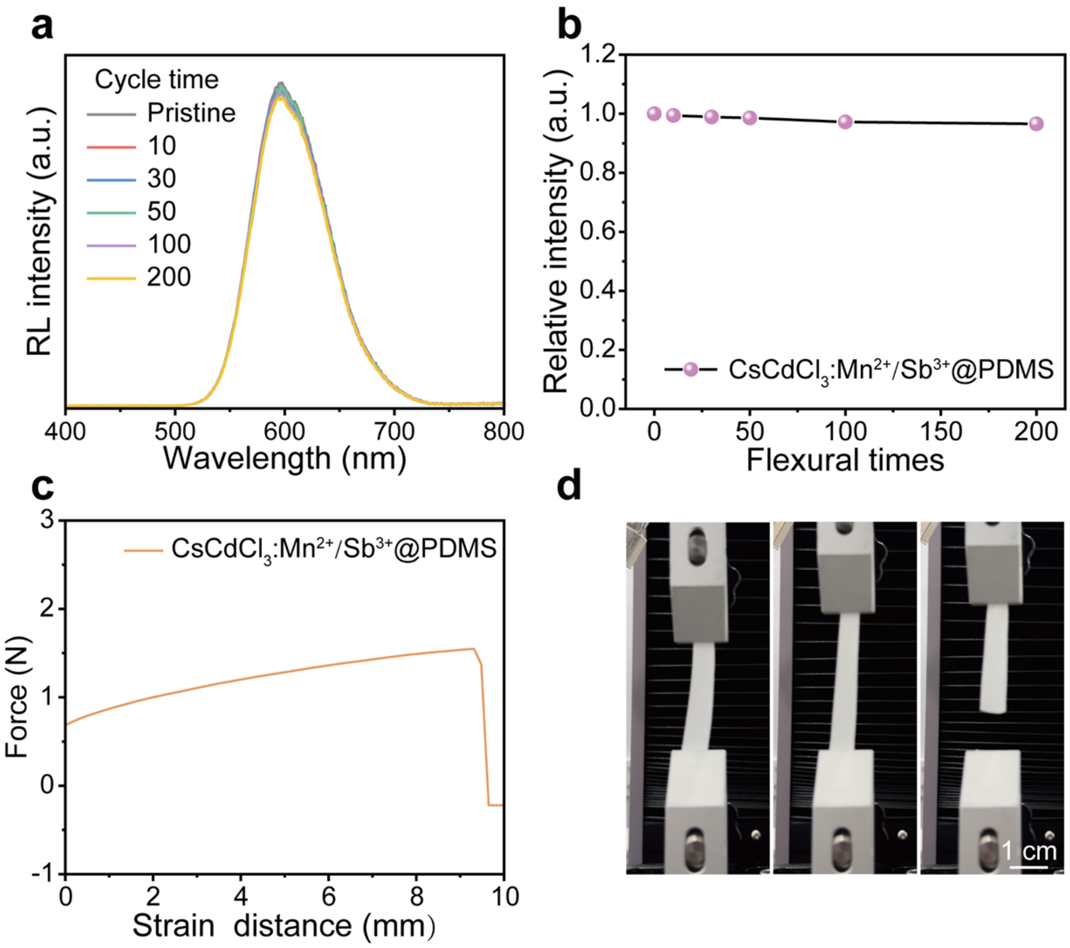

Figure S15. Flexural and tensile tests of flexible scintillation screens. (a-b) Comparison of radioluminescence intensity of the flexible scintillator screen after bending at different times. (c-d) Tensile testing of the flexible scintillator screen of $CsCdCl_3$:Mn^{2+}/Sb^{3+}@PDMS (width 7mm, length 6cm, thickness 100mm).